



Fiber-optic wireless sensor network using ultra-weak fiber Bragg gratings for vertical subsurface deformation monitoring

Su-Ping Liu¹ · Bin Shi¹ · Kai Gu¹ · Cheng-Cheng Zhang¹ · Jian-Hui He¹ · Jing-Hong Wu² · Guang-Qing Wei³

Received: 22 January 2021 / Accepted: 6 July 2021 / Published online: 22 July 2021
© The Author(s), under exclusive licence to Springer Nature B.V. 2021

Abstract

The determination of subsurface deformation is critical to understanding the subsurface dynamic processes, but most of conventional monitoring methods still have challenges in remotely obtaining detailed data. Herein, a novel fiber-optic wireless sensor network using the ultra-weak fiber Bragg gratings technique was proposed. It allows real-time remote capture of subsurface deformation along the fiber-optic cables. Such a fiber-optic measurement system was employed in a borehole to a depth of 340 m in Cangzhou, China. Strain profiles were measured monthly with a spatial resolution of 5 m and strain resolution of 1 $\mu\epsilon$, and the development of all strata deformation in the aquifer systems was calculated from January 2019 to December 2019. It turns out that the subsidence rate in this area is approximate 9 mm/a, which agrees well with the result of extensometer measurements. The significant strata compaction in the second aquifer and the third aquitard rapidly increased from May 2019 to July 2019, which could be attributed to the decline in groundwater. It is concluded that the fiber-optic wireless sensor network accurately captures subsurface deformation development and helps to better elucidate the subsurface deformation mechanism and provide solutions for the prevention and mitigation.

Keywords Real-time monitoring · Subsurface deformation · Wireless sensor network · Ultra-weak fiber Bragg gratings

✉ Bin Shi
shibin@nju.edu.cn

✉ Kai Gu
gukai@nju.edu.cn

Su-Ping Liu
liusuping@smail.nju.edu.cn

¹ School of Earth Sciences and Engineering, Nanjing University, Nanjing 210023, China

² School of Civil Engineering, Suzhou University of Science and Technology, Suzhou 215011, China

³ Suzhou NanZee Sensing Technology Ltd., Suzhou 215123, China

1 Introduction

Ground deformation is one feature of the geohazards, e.g., earthquake, landslides, and land subsidence (Amelung et al. 1999; Hu et al. 2020; Parker et al. 2011; Xu et al. 2020). It may damage the existing geological landscape and artificial infrastructures and threaten human life and properties. Monitoring the dynamic process of vertical ground deformation is critical to understanding the disaster mechanisms. The conventional monitoring methods can be categorized into space-based techniques (including InSAR and airborne LiDAR) and ground-based techniques (including GNSS, LiDAR, leveling, and extensometers) (Amelung et al. 1999; Galloway and Burbey 2011; Hu et al. 2020; Hung et al. 2017; Xu et al. 2020). While most of these techniques can only detect the surface motions, groups of extensometers in boreholes allow the determination of subsurface deformation at several depths, but the spatial resolution in measurement can range from tens to hundreds of meters, e.g., 30–328 m in Yang et al. (2019). Therefore, it remains challenging to map the detailed distribution of vertical subsurface deformation using conventional monitoring methods due to the spatially discrete displacements information.

Fiber-optic sensing (FOS) is an advanced investigation method for geological disasters with the advantages of long-distance, spatially continuous, and robust measurement. In recent years, FOS technology has been implemented in distributed strain sensing (DSS) (Kogure and Okuda 2018; Liu et al. 2021), distributed temperature sensing (DTS) (Freifeld et al. 2008; Selker et al. 2006), and distributed acoustic sensing (DAS) (Lindsey et al. 2017; Marra et al. 2018) in geoscience, hydraulic and geotechnical engineering. Among these technologies, DSS technologies are usually based on Brillouin scattering or Rayleigh scattering, which enable strain measurements in the meter- or centimeter-scale spatial resolutions, respectively (Barrias et al. 2016). DSS adopts a strain-sensing fiber-optic cable to determine the strain profile along the entire length, which can be used to quantify the deformation of strata or infrastructures. The feasibility of DSS for subsurface deformation monitoring in boreholes has been illustrated in previous studies (Gu et al. 2018; Kokubo et al. 2015; Liu et al. 2019; Liu et al. 2020; Wu et al. 2015; Zhang et al. 2018). More recently, the utilization of micro-anchored cables significantly improved the quality of fiber-optic measurements in the near-surface (Zhang et al. 2021a).

However, most of the long-distance DSS techniques are manual measurements accompanied by low automation and intelligence features. The fixed and low sampling frequencies limited observation data that are not conducive to exploring the subsurface deformation mechanisms. Some researchers utilized fiber Bragg grating (FBG) sensors to wirelessly monitor the dynamic strain with a short time interval (Kim et al. 2013; Saouma et al. 1998; Yao et al. 2015). With the development of ultra-weak fiber Bragg gratings (UWFBGs) technology, it was used to improve the capacity of Bragg gratings in a fiber-optic cable (Muanenda et al. 2019; Wang et al. 2015; Wang et al. 2011). Such technology offers the possibility of remote real-time DSS for subsurface deformation.

In this study, a new type of strain measurement technology using UWFBGs is proposed, allowing remote monitoring of subsurface deformation. Based on this, the fiber-optic wireless sensor network was proposed, and the subsurface strain profiles in Cangzhou, China, from January 2019 to December 2019 were demonstrated with a spatial resolution of 5 m and a strain resolution of 1 $\mu\epsilon$. The fiber-optic measured strata deformation was verified by the results measured by extensometers. The fiber-optic measurements show potential for revealing subsurface deformation processes and early warning systems in geoscience.

2 Methodology

2.1 Fiber Bragg grating technique

As shown in Fig. 1, a fiber Bragg grating (FBG) with a period of Λ is written in the fiber core. The FBG will reflect the light of a specific wavelength when the broadband light is injected into the fiber and passes through the FBG. The Bragg wavelength λ_B of the reflected light is determined by the grating period Λ and the effective refractive index n_{eff} of grating in the fiber core by (Hill and Meltz 1997):

$$\lambda_B = 2n_{eff}\Lambda \tag{1}$$

The Bragg wavelength will shift when the axial strains $\Delta\varepsilon$ and temperature variations ΔT are applied to the fiber-optic. Moreover, the Bragg wavelength shifts ($\Delta\lambda_B$) keep a linear relationship with the strain or temperature changes as follows (Moyo et al. 2005):

$$\frac{\Delta\lambda_B}{\lambda_B} = K_\varepsilon \Delta\varepsilon \tag{2}$$

$$\frac{\Delta\lambda_B}{\lambda_B} = K_T \Delta T \tag{3}$$

where the K_ε and K_T are the wavelength sensitivity coefficients of strain and temperature, respectively. The two coefficients can be, respectively, calibrated by laboratory experiments at constant temperature or without strain. Generally, the FBGs are more sensitive to the change of strain, e.g., the K_ε and K_T of 1550 nm FBGs are ~ 1.15 pm/ $\mu\varepsilon$ and ~ 14 pm/ $^\circ\text{C}$, respectively (Rao 1997).

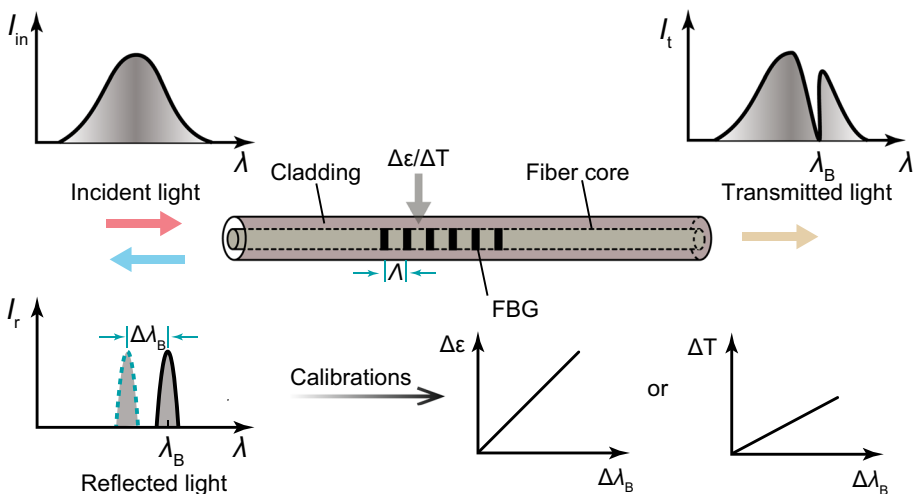


Fig. 1 Principle of fiber Bragg grating measurement

2.2 UWFBG-based strain measurement

To improve the capacity of Bragg gratings in a fiber-optic cable, the ultra-weak fiber Bragg gratings (UWFBGs) technique was proposed by decreasing the refractive index R of the Bragg gratings (Muanenda et al. 2019; Wang et al. 2015; Wang et al. 2011). Thousands of Bragg gratings with ultra-weak refractive index (i.e., $R \leq 0.1\%$) can be written in the same fiber core, respectively, and each UWFBG can measure a strain or temperature result. Based on time-division multiplexing (TDM) technology, all UWFBGs can be localized when massive UWFBGs are connected in series because their reflection time of the incident light varies at different positions (Fig. 2). Therefore, a series of UWFBGs with the same refractive index and wavelength ($\lambda_1 = \lambda_2 = \dots = \lambda_n$) can be multiplexed in a fiber core, namely the identical UWFBGs array. Finally, the reflected time is used to localize the sensors (Eq. (4)) and the wavelength shifts are used to obtain the strain or temperature changes.

$$t = \frac{2n_{\text{eff}}d}{c} \tag{4}$$

where c is the light velocity in the fiber-optic; d is the interval distance of UWFBGs; t is the time interval between receiving two UWFBGs wavelengths in the fiber.

Compared to the Brillouin scattering- or Rayleigh scattering-based DSS techniques, the UWFBGs technique can record and remotely transmit the strain results, and the time interval of data sampling for field monitoring can be as intensive as 1 min. The others belong to the manual survey techniques, so the in-situ measurement and the data storage are conducted manually. Usually, the fixed and low sampling frequencies are the apparent features, and the sampling frequencies of the DSS technique may range from 3 to 5 months in the long-term monitoring (Liu et al. 2019; Liu et al. 2020).

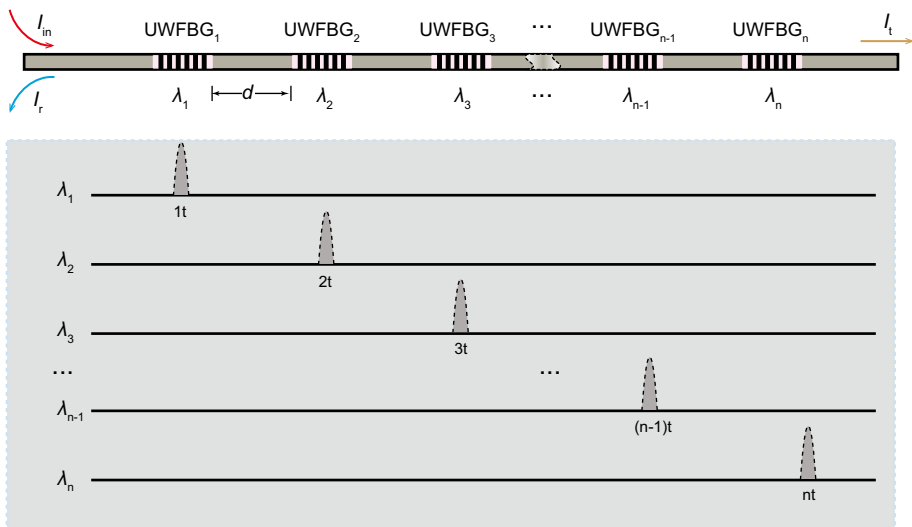


Fig. 2 Distributed strain sensing based on UWFBGs array

2.3 Strain integration methods

For distributed strain sensing cable (DSS cable, Fig. 3a), the soil strain transfer along the entire length in cable and soil deformation can be calculated by

$$\Delta L = \int_{l_1}^{l_2} \epsilon(l)dl \tag{5}$$

where ΔL is the deformation from l_1 to l_2 , and ϵ is the strain along the cable.

For strain sensing cable with UWFBGs (UWFBG cable, Fig. 3b), only the glued point inside the cable can respond to soil strain because the other segments are not in contact with the cable sheath. Hence, the deformation of the cable can be calculated by

$$\Delta H = \int_{H_1}^{H_2} \epsilon(H)dH = (H_2 - H_1) \cdot \epsilon(H) \tag{6}$$

where ΔH is the deformation from H_1 to H_2 , and $\epsilon(H)$ is a single-point strain of UWFBG between H_1 and H_2 . The fiber-optic is glued at two sides of UWFBG with a constant interval.

2.4 Fiber-optic wireless sensor network

Fiber-optic wireless sensor network allows fiber-optic sensors to monitor and remotely transmit the target results, mainly including strain or temperature. For example, the network can host a massive number of UWFBGs strain sensors installed into the boreholes or trenches in the study area, and then a detailed strain profile can be captured. Figure 4 illustrates the framework of the fiber-optic wireless sensor network. The prior work is surveying the geological environment based on the Space-Sky-Ground (S-S-G) techniques (Hu et al. 2020; Xu et al. 2020), followed by determining the study area and the hotspot case. Then, the single- or multi-parameter fiber-optic wireless sensors will be installed in the field (sensing module). The real-time fiber-optic measurement results are interpreted by the fiber-optic interrogators and then remotely transmitted to the software in the host via the 4/5G Internet within 10 s (transmission module). In the cloud module, the software receives the wavelength measured by UWFBGs,

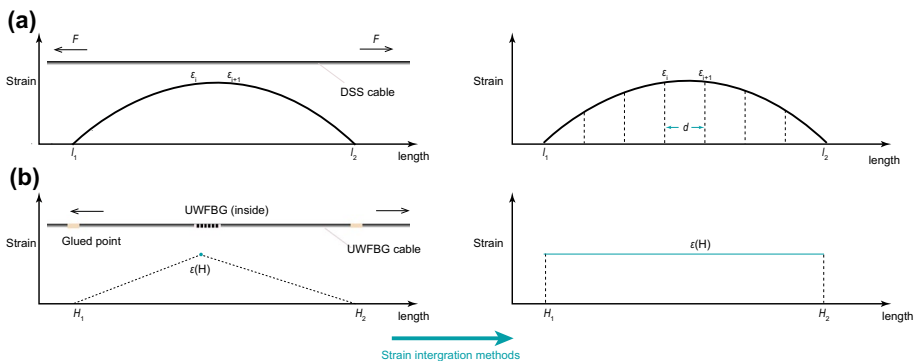


Fig. 3 Typical tensile strain distribution of fiber-optic cables induced by soil. **a** DSS cable. **b** UWFBG cable

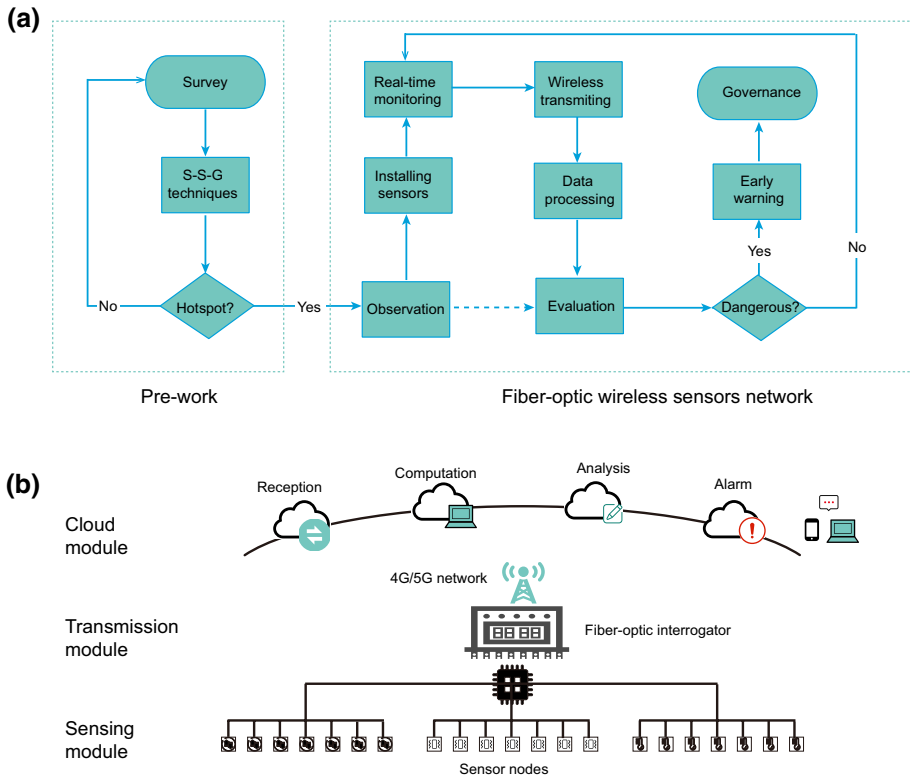


Fig. 4 The framework of the fiber-optic wireless sensor network **a** Flowchart of early warning system via fiber-optic wireless sensor network **b** Three modules of fiber-optic wireless sensor network including the sensing, transmission, and cloud modules

calculates the target results, analyzes the critical state, and finally decides whether to warn or not (Fig. 4b).

As shown in Fig. 5a, a borehole-based fiber-optic wireless sensor network is employed for vertical strain measurement: (i) a strain sensing cable with UWFBGs is installed into the borehole (Fig. 5b, c), which works as the sensing module for soil strain; (ii) In transmission module, the wavelength interpreted by the UWFBG interrogator can be remotely transmitted to the control center via 4G/5G Internet (Fig. 5d); (iii) The software outputs the strain profile and the subsurface deformation (Fig. 5e); (iv) Furthermore, the warning algorithm should be integrated into the cloud module, for example, comparing the vertical subsurface deformation to the historical data, analyzing the strata deformation state, and publishing the early warning if a certain threshold is exceeded.

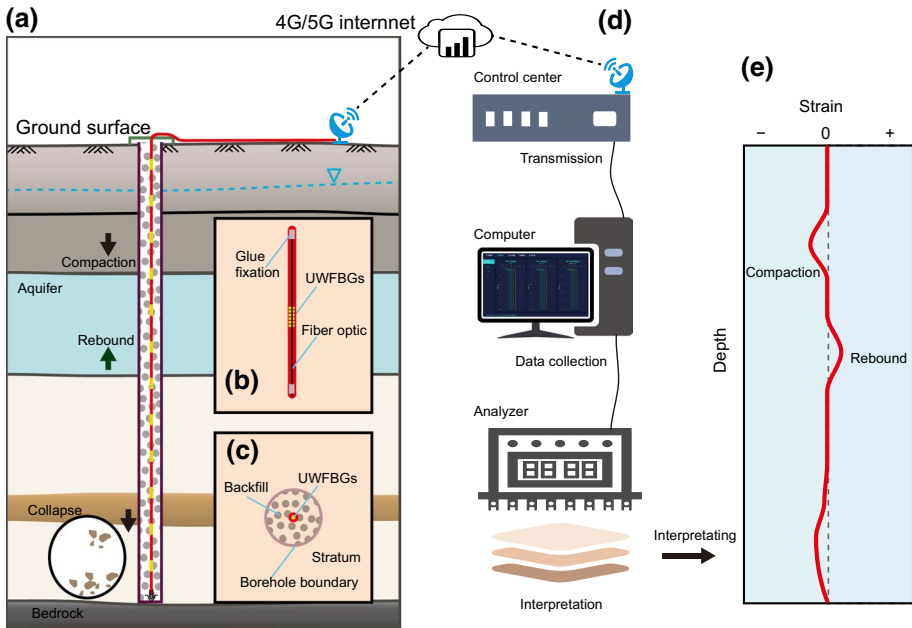


Fig. 5 Schematic view of the wireless-sensing system of subsurface deformation. **a** The borehole-based monitoring system of strata deformation using UWFBGs; **b** Front view of strain sensing cable with UWFBGs; **c** Cross-sectional view of borehole; **d** Data transmission, collection, and interpretation; **e** Vertical strain measurement results

3 Fiber-optic measurements of vertical subsurface deformation in Cangzhou

The fiber-optic wireless sensor network was deployed in Cangzhou, North China Plain, China, which undergoes severe land subsidence (Xue et al. 2005). Figure 6 shows the location of the study area and accumulative subsidence of the Beijing–Tianjin–Hebei Plain. The land subsidence in Cangzhou occurred in the 1970s, and the maximum accumulative subsidence in the urban area reached 2.5 m in 2008, and the average subsidence rate exceeded 65 mm/a (Xue et al. 2005; Zhu and Guo 2014). Approximately 15% area undergoes accumulative subsidence greater than 1 m. The subsidence rate dropped to 10–15 mm/a with the prohibition of groundwater extraction in 2005. Previous studies show that the land subsidence in Cangzhou is mainly caused by groundwater exploitation in the third aquifer, which causes the cohesive soil layer (clay and silty clay) to be compacted and difficult to recover (Guo et al. 2015; Zhu and Guo 2014).

The borehole (38°17'20" N, 116°52'30" E), namely CZ01, with a depth of 340 m and a diameter of 129 mm was drilled on 20 September 2018 (Fig. 7). The strata lithology is dominated by silty clay, clay, silt, and silty sand. The Quaternary deposit is divided into four aquifer–aquitard layers, and the fourth aquifer is not fully exposed due to the limitation of the CZ01 borehole depth.

The fiber-optic cable with UWFBGs used in the study is the NZS-DDS-C03 cable (Suzhou Nanzee Sensing, China). From outside to inside, the loose-buffered cable consists of a polyurethane (PE) jacket, steel conduit, buffer, UWFBGs, and silica fiber-optic

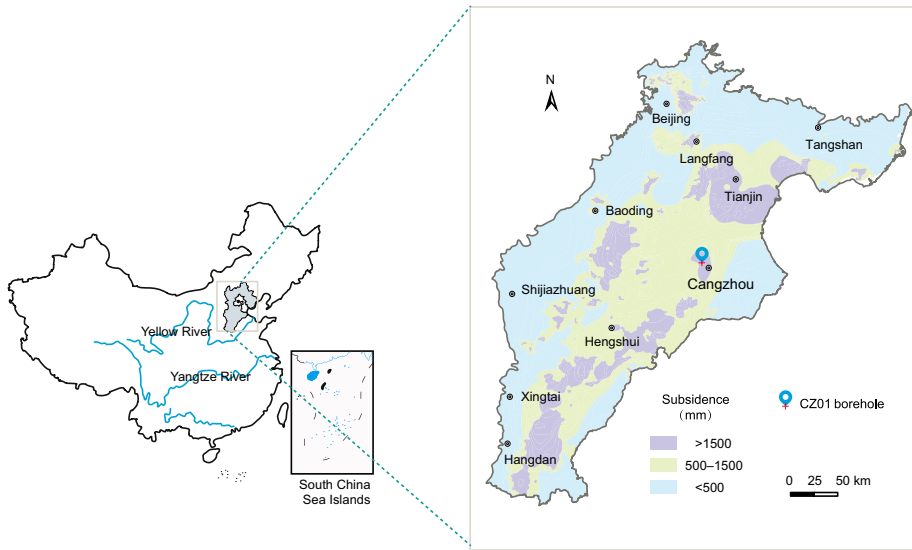


Fig. 6 The location of the CZ01 borehole and the accumulative subsidence map of the study area

(Fig. 8). Note that the manufactured UWFBG cable is the identical UWFBG array, and the interval of UWFBGs is 5 m. Before the field investigation, the UWFBG cable should be calibrated for the strain sensitivity coefficients. A 3-m-long fiber-optic cable with a UWFBG was cut from the same UWFBG cable and then glued with an interval of 2 m, and finally calibrated in the laboratory. As shown in Fig. 9, the cable is horizontally fixed at the calibration tester with a length of 2 m, which can be extended by the motor with a certain velocity. The fiber-optic wavelength interrogator measures the wavelength results after each displacement increment of 2 mm. The NZS-QDS-Q01 UWFBG interrogator analyzes the wavelengths, and its technical specifications are summarized in Table 1. Finally, the strain coefficient can be calculated by Eq. (2), and the strain coefficient calibrated in this research is $869.56 \mu\epsilon/\text{nm}$ (Fig. 10).

4 Results and validation

4.1 Subsurface strain profile

High-resolution subsurface strain profiles shed light on the subsurface deformation. For the fiber-optic measurement in the CZ01 borehole, the strain can be transferred from the wavelength measured using the UWFBG cable; the wavelengths were analyzed and transmitted remotely by the NZS-QDS-Q01 UWFBG interrogator placed in the observatory near the CZ01 borehole. Figure 11a shows 11-month wavelength results from January 2019 to December 2019, and Fig. 11b depicts vertical strain profiles along the CZ01 borehole. To better elucidate the subsurface deformation process, a color map showing the full-depth (340 m) strain changes is shown in Fig. 11c. It can be readily seen that the negative strain dominates the soil strain, while the positive strain occurs in only three minor layers. The first stratum with the positive strain is localized at the shallow depth of 5 m,

Fig. 7 Subsurface deformation measurement using UWFBG-based fiber-optic wireless sensor network in the CZ01 borehole

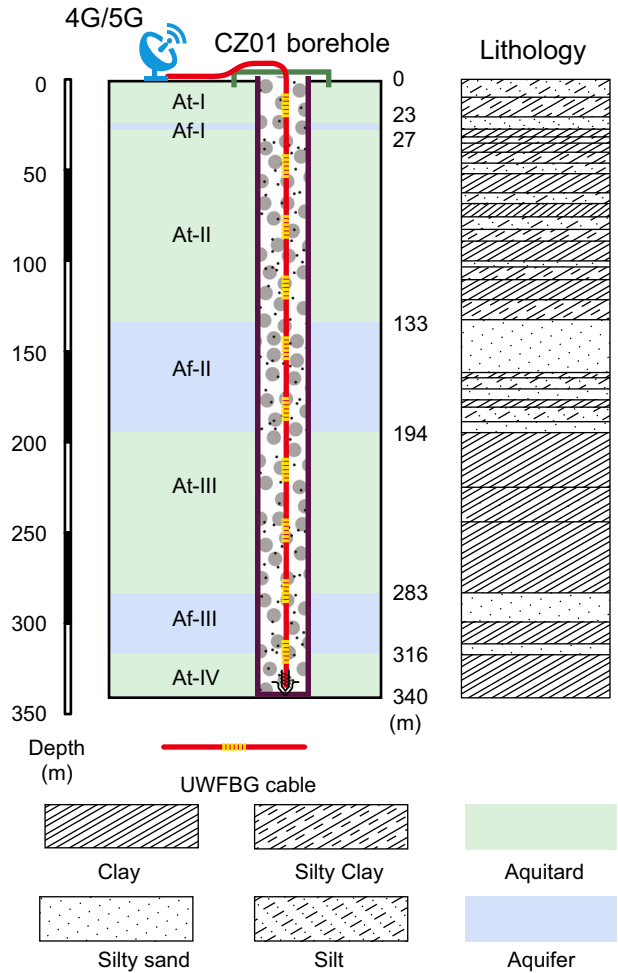
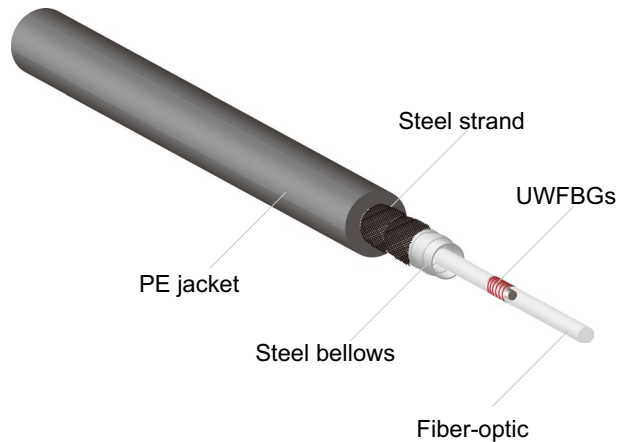


Fig. 8 Schematic view of strain sensing cable with UWFBGs, from outside to inside, PE jacket, steel strand, steel bellows, UWFBGs, and fiber-optic



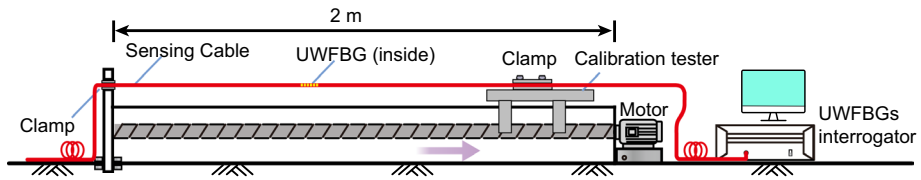
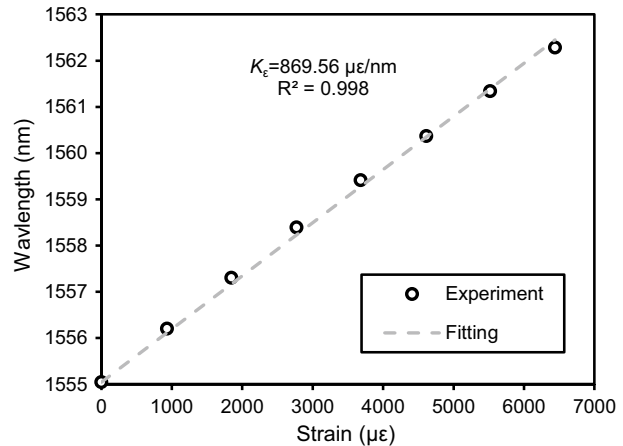


Fig. 9 Schematic view of strain-based calibration instrument, including pullout motor, calibration tester, and monitoring and optical interrogator

Fig. 10 Calibration results of the UWFBG cable



which can be attributed to the variations of air and shallow soil temperature (Kogure and Okuda 2018; Zhang et al. 2018). The second layer undergoing the positive strain (slight, $\sim 50 \mu\epsilon$) appears at a depth of 44–54 m. A third positive-strain stratum can be easily found at a depth of 281–286 m in the third aquifer (Af-III), which means the rebound occurring in the Af-III. The rebound of aquifers is a normal feature that has been reported in many regions, e.g., the Yangtze River Delta Plain (Wu et al. 2015) and the North China Plain (Guo et al. 2015). While the rebound occurs locally, the compaction is the significant pattern of subsurface deformation in the CZ01 borehole.

To summarize, the fiber-optic wireless sensor network was successfully implemented in the CZ01 borehole, and the detailed strain profiles were captured in depth and time. However, the reliability of the strain results is still unknown, the next section will introduce the comparison with results from extensometers.

4.2 Deformation validation

For fiber-optic measurements, the subsurface deformation can be calculated by Eq. (6). Meanwhile, the strata deformation can also be obtained by monitoring the displacement between two extensometers, and three borehole-based extensometers were installed near the CZ01 borehole at a depth of 41 m, 150 m, and 267 m, respectively. The strata deformation results calculated by UWFBG cable and extensometers are shown in Fig. 12, positive values mean the rebound, while negative values mean compaction. Only two strata deformation with the thickness of 57 and 127 m are compared, respectively. It is evident that

Table 1 Technical specifications of UWFBG interrogator

Operation wavelength (nm)	Channels	UWFBGs/channel	Resolution (pm)	Spatial resolution (m)	Measurement length (km)	Sampling time (min)
1525–1565	16	> 2000	1	≥ 0.5	≤ 20	≤ 1

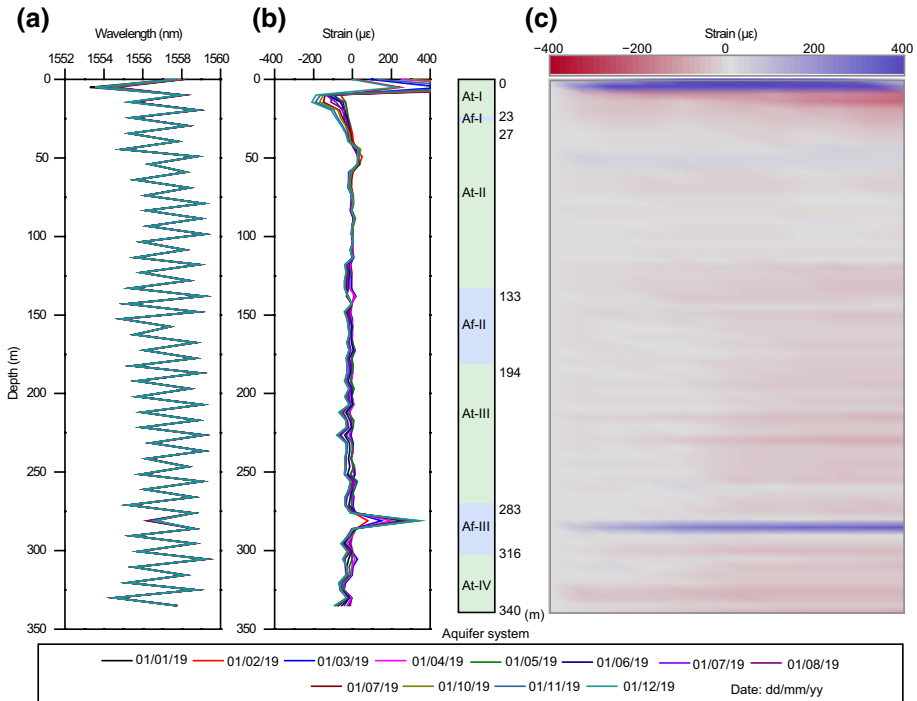


Fig. 11 CZ01 borehole: 11 months optically measured subsurface strain profile from 1 January 2019 to 1 December 2019. **a** Real-time wavelength change results; **b** Strain profiles; **c** Color map of subsurface strain changes. Positive values mean rebound; negative values mean compaction

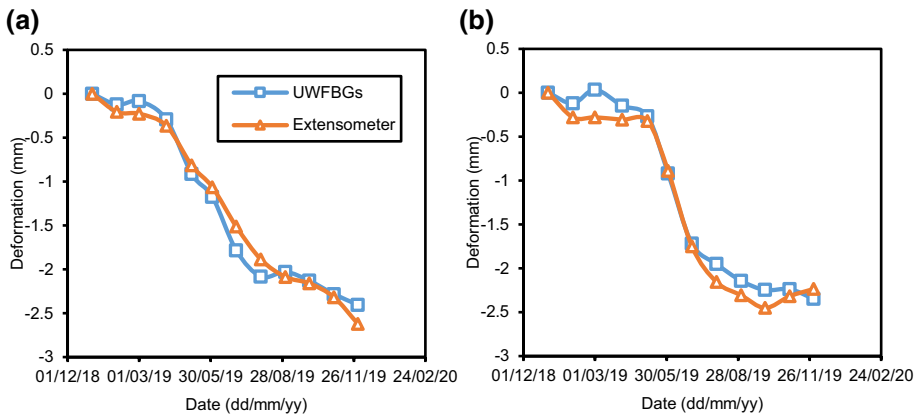


Fig. 12 UWFBGs and extensometers measured strata deformation in the CZ01 borehole at a depth of **a** 41–150 m and **b** 150–267 m

fiber-optic measurement is in good agreement with extensometers in the trend and magnitude of the subsurface deformation at a depth of 41–150 m and 150–267 m, respectively (Fig. 12a, b), with cumulative strata compaction of ~2.5 mm. Note that the slight rebound

in the second aquitard (At-II) was neglected in the compaction behavior of the 109-m-thick stratum (41–150 m deep). Clearly, the UWFBG measurement accurately maps the detailed subsurface deformation and avoids the underestimation of strata compaction.

4.3 Sensitivity to groundwater

With the strain profiles along the entire length, the significant deformation of the aquifer system from approximately 10–340 m depth can be easily obtained. Note that strata deformation below 10 m is subtracted for the effects of air temperature, and the influence of deeper strata temperature on UWFBGs can be ignored in the field investigation. Figure 13 shows the relationship between groundwater level and strata deformation, including four aquitards and three aquifers at a depth of 10–23 m (At-I), 27–133 m (At-II), 194–283 m (At-III), 316–340 m (At-IV), 23–27 m (Af-I), 133–194 m (Af-II) and 283–316 m (Af-III), respectively. Ongoing subsidence was observed in 2019, reaching cumulative subsidence of 9.0 mm. The deformation rate dropped to the lowest value (–2.5 mm/month) in July 2019 and then increased and tended to be stable (approximate –0.8 mm/month) (Fig. 13a). Meanwhile, the groundwater level decreased to 95 m due to the peak water consumption in the summer (Fig. 13b). Therefore, the subsidence rate keeps a correlation with fluctuations in deep groundwater. From Fig. 13c, the compression of the At-III increased significantly in July 2019, and the monthly subsidence reached ~0.9 mm; after October 2019, the compression gradually stabilized and reached 2.9 mm. The strata deformation of the At-III coincided with the groundwater fluctuations. As shown in Fig. 13d, both compression and rebound (≤ 2 mm) were found in aquifers, the adjacent aquifer (Af-II) over the At-III showed a similar tendency of deformation. Note that the Af-III rebounded when the groundwater level decreased, indicating that the rebound might be dominated by deeper groundwater.

Generally, the subsidence in Cangzhou has been controlled, and its rate tends to be stable, which is within the reasonable subsidence range according to the historical data. This indicates that the early warning is not necessary.

5 Prospect on fiber-optic wireless sensor network

The traditional subsurface deformation measurements comprise only several layers in the aquifer system. Recently, the emerging fiber-optic sensing technologies show the potential in borehole-based distributed strain sensing, which contributes to identifying the hotspots of subsurface deformation. For example, Liu et al. (2019) and Liu et al. (2020) deployed the DSS cables into boreholes to capture the strata strain response to the groundwater fluctuations and high buildings at 3–5 months intervals in Lianyungang and Tianjin, China, respectively, and investigated the land subsidence mechanisms. Herein, the UWFBGs technique supplements the DSS technique that allows real-time remote strain measurement. The UWFBG measured results are in good agreement with the extensometer results in millimeters scale, which indicates that the UWFBG cable maintains a strong cable-soil interaction in the CZ01 borehole and accurately transfers strata strain. The robustness of strain-based fiber-optic wireless sensor network and the reliability of measured subsurface deformation have been demonstrated in this study. Thus the following work can be conducted as follows:

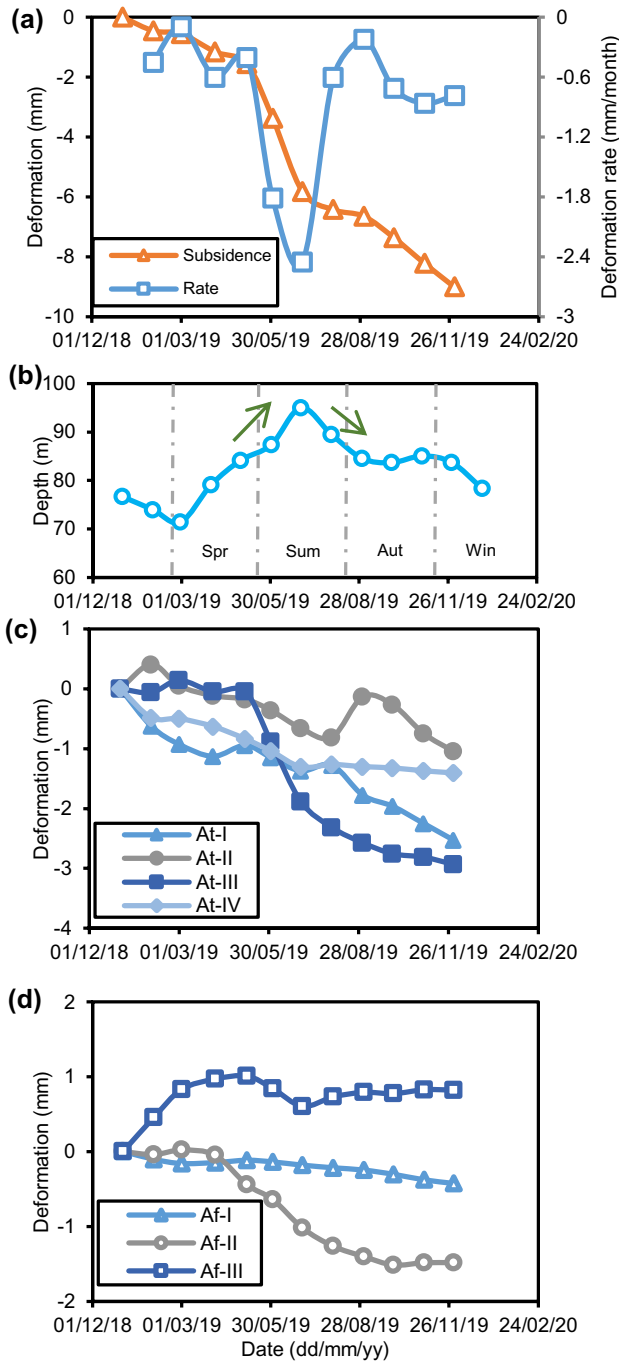


Fig. 13 CZ01 borehole: Sensitivity of strata deformation to groundwater changes. **a** Accumulative subsidence. **b** The groundwater level in Cangzhou. Spr: Spring; Sum: Summer; Aut: Autumn; Win: Winter. **c** Four aquitards deformation and **d** three aquifers deformation measured by UWFBGs

1. The prediction of subsurface deformation based on machine learning. The fiber-optic wireless sensors network can output the reliable strain data in 1 min in the cloud module. The massive strain data are stored and calculated in the software and would be a database for the precise prediction of subsurface deformation if the machine learning method could be integrated into the software. A similar approach has been implemented in the landslide early warning system, e.g., Xu et al. (2020) and Zhang et al. (2021b).
2. Wireless sensors network of multi-parameter. UWFBG sensors are sensitive to strain and temperature, which helps obtain the other related environmental parameters using the specific transfer functions. Therefore, the UWFBG sensor will be manufactured to measure stress, salinity, moisture, and vibration (Bai et al. 2017; Jiang et al. 2021; Zhu et al. 2017), enriching the fiber-optic sensing system in the future.

6 Conclusions

In this study, a fiber-optic wireless sensor network with UWFBGs was proposed, and the fiber-optic measurements for subsurface deformation in Cangzhou, North China Plain, China, was demonstrated. The findings are drawn as follows:

1. The fiber-optic wireless sensors network using UWFBGs for monitoring subsurface deformation is firstly reported. Such a novel network can remotely transmit wavelength results in almost real-time and provide near full-length strain profiles of the subsurface.
2. The proposed fiber-optic network was successfully implemented and efficient in mapping the subsurface deformation in Cangzhou, China. The annual land subsidence in this area was 9.0 mm in 2019, which agreed well with the result of extensometers.
3. The detailed subsurface deformation results help identify the dominant compressed strata and drivers. The Af-II and At-III in the aquifer system significantly contributed to the land subsidence. The deformation of these strata varied with groundwater fluctuations: the land subsidence rapidly increased from May 2019 to July 2019 due to the decline in groundwater.
4. Furthermore, the fiber-optic wireless sensors network possesses the potential for intelligent database and networking. The UWFBGs sensors can be developed toward sensing strain- or temperature-based parameters in geosciences with high accuracy.

Acknowledgements This work was supported by the National Natural Science Foundation of China Grants (42030701, 41977217, and 41427801), the Natural Science Foundation of Jiangsu Province Grant (BK20200217), and the China Scholarship Council Grant (201906190153). The authors would like to thank Wen-Xuan Zhang from Suzhou NanZee Sensing Ltd. and all those from Hebei Survey Institute of Environmental Geology who were involved in the fiber-optic measurements in the Cangzhou for their technical assistance.

Declarations

Conflicts of interest The authors declare that they have no conflict of interest.

References

- Amelung F, Galloway DL, Bell JW, Zebker HA, Laczniak RJ (1999) Sensing the ups and downs of Las Vegas: InSAR reveals structural control of land subsidence and aquifer-system deformation. *Geology* 27:483–486. [https://doi.org/10.1130/0091-7613\(1999\)027<0483:STUADO>2.3.CO;2](https://doi.org/10.1130/0091-7613(1999)027<0483:STUADO>2.3.CO;2)
- Bai W, Yang M, Hu C, Dai J, Zhong X, Huang S, Wang G (2017) Ultra-weak fiber Bragg grating sensing network coated with sensitive material for multi-parameter measurements. *Sensors* 17:1509. <https://doi.org/10.3390/s17071509>
- Barrias A, Casas JR, Villalba S (2016) A review of distributed optical fiber sensors for civil engineering applications. *Sensors* 16:748. <https://doi.org/10.3390/s16050748>
- Freifeld BM, Finsterle S, Onstott TC, Toole P, Pratt LM (2008) Ground surface temperature reconstructions: using in situ estimates for thermal conductivity acquired with a fiber-optic distributed thermal perturbation sensor. *Geophys Res Lett* 35: L14309. <https://doi.org/10.1029/2008gl034762>
- Galloway DL, Burbey TJ (2011) Review: regional land subsidence accompanying groundwater extraction. *Hydrogeol J* 19:1459–1486. doi:<https://doi.org/10.1007/s10040-011-0775-5>
- Gu K, Shi B, Liu C, Jiang H, Li T, Wu J (2018) Investigation of land subsidence with the combination of distributed fiber optic sensing techniques and microstructure analysis of soils. *Eng Geol* 240:34–47. <https://doi.org/10.1016/j.enggeo.2018.04.004>
- Guo H, Zhang Z, Cheng G, Li W, Li T, Jiao JJ (2015) Groundwater-derived land subsidence in the North China Plain. *Environ Earth Sci* 74:1415–1427. <https://doi.org/10.1007/s12665-015-4131-2>
- Hill KO, Meltz G (1997) Fiber Bragg grating technology fundamentals and overview. *J Lightwave Technol* 15:1263–1276. <https://doi.org/10.1109/50.618320>
- Hu X, Burgmann R, Schulz WH, Fielding EJ (2020) Four-dimensional surface motions of the Slumgullion landslide and quantification of hydrometeorological forcing. *Nat Commun* 11:2792. <https://doi.org/10.1038/s41467-020-16617-7>
- Hung W-C et al (2017) Land subsidence in Chiayi, Taiwan, from compaction well, leveling and ALOS/PALSAR: aquaculture-induced relative sea level rise. *Remote Sens* 10:40. <https://doi.org/10.3390/rs10010040>
- Jiang J et al (2021) Real-time monitoring method for unauthorized working activities above the subway tunnel based on ultra-weak fiber Bragg grating vibration sensing array. *Measurement* 182:109744. <https://doi.org/10.1016/j.measurement.2021.109744>
- Kim J-T, Nguyen K-D, Huynh T-C (2013) Wireless health monitoring of stay cable using piezoelectric strain response and smart skin technique. *Smart Struct Syst* 12:381–397. https://doi.org/10.12989/sss.2013.12.3_4.381
- Kogure T, Okuda Y (2018) Monitoring the vertical distribution of rainfall-induced strain changes in a landslide measured by distributed fiber optic sensing with Rayleigh backscattering. *Geophys Res Lett* 45:4033–4040. <https://doi.org/10.1029/2018gl077607>
- Kokubo T, Takenobu K, Ikeda H, Kunisue S, Nohara D, Ooba K (2015) In-situ volume change monitoring for deep underlay strata with fiber optical technology. In: ISRM VietRock International Workshop. International Society for Rock Mechanics and Rock Engineering
- Lindsey NJ et al (2017) Fiber-optic network observations of earthquake wavefields. *Geophys Res Lett* 44:11792–11799. <https://doi.org/10.1002/2017gl075722>
- Liu J et al (2019) Monitoring of vertical deformation response to water draining–recharging conditions using BOFDA-based distributed optical fiber sensors. *Environ Earth Sci* 78:406. <https://doi.org/10.1007/s12665-019-8409-7>
- Liu S-P, Gu K, Zhang C-C, Shi B (2021) Experimental research on strain transfer behavior of fiber-optic cable embedded in soil using distributed strain sensing. *Int J Geomech*. [https://doi.org/10.1061/\(ASCE\)GM.1943-5622.0002155](https://doi.org/10.1061/(ASCE)GM.1943-5622.0002155)
- Liu S-P, Shi B, Gu K, Zhang C-C, Yang J-L, Zhang S, Yang P (2020) Land subsidence monitoring in sinking coastal areas using distributed fiber optic sensing: a case study. *Nat Hazards* 103:3043–3061. <https://doi.org/10.1007/s11069-020-04118-1>
- Marra G et al (2018) Ultrastable laser interferometry for earthquake detection with terrestrial and submarine cables. *Science* 361:486–490. <https://doi.org/10.1126/science.aat4458>
- Moyo P, Brownjohn JMW, Suresh R, Tjin SC (2005) Development of fiber Bragg grating sensors for monitoring civil infrastructure. *Eng Struct* 27:1828–1834. <https://doi.org/10.1016/j.engstruct.2005.04.023>
- Muanenda Y, Faralli S, Oton CJ, Cheng C, Yang M, Di Pasquale F (2019) Dynamic phase extraction in high-SNR DAS based on UWFBGs without phase unwrapping using scalable homodyne demodulation in direct detection. *Opt Express* 27:10644–10658. <https://doi.org/10.1364/OE.27.010644>

- Parker RN et al (2011) Mass wasting triggered by the 2008 Wenchuan earthquake is greater than orogenic growth. *Nat Geosci* 4:449–452. <https://doi.org/10.1038/ngeo1154>
- Rao Y-J (1997) In-fibre Bragg grating sensors. *Meas Sci Technol* 8:355–375. <https://doi.org/10.1088/0957-0233/8/4/002>
- Saouma VE, Anderson DZ, Ostrander K, Lee B, Slowik V (1998) Application of fiber Bragg grating in local and remote infrastructure health monitoring. *Mater Struct* 31:259–266. <https://doi.org/10.1007/BF02480424>
- Selker J, van de Giesen N, Westhoff M, Luxemburg W, Parlange MB (2006) Fiber optics opens window on stream dynamics. *Geophys Res Lett* 33: L24401. <https://doi.org/10.1029/2006gl027979>
- Wang C, Shang Y, Liu XH, Wang C, Yu HH, Jiang DS, Peng GD (2015) Distributed OTDR-interferometric sensing network with identical ultra-weak fiber Bragg gratings. *Opt Express* 23:29038–29046. <https://doi.org/10.1364/OE.23.029038>
- Wang Y, Gong J, Wang DY, Dong B, Bi W, Wang A (2011) A quasi-distributed sensing network with time-division-multiplexed fiber Bragg gratings. *IEEE Photon Technol Lett* 23:70–72. <https://doi.org/10.1109/lpt.2010.2089676>
- Wu J, Jiang H, Su J, Shi B, Jiang Y, Gu K (2015) Application of distributed fiber optic sensing technique in land subsidence monitoring. *J Civ Struct Health Monitor* 5:587–597. <https://doi.org/10.1007/s13349-015-0133-8>
- Xu Q et al (2020) Successful implementations of a real-time and intelligent early warning system for loess landslides on the Heifangtai terrace, China. *Eng Geol* 278: 105817. <https://doi.org/10.1016/j.enggeo.2020.105817>
- Xue Y-Q, Zhang Y, Ye S-J, Wu J-C, Li Q-F (2005) Land subsidence in China. *Environ Geol* 48:713–720. <https://doi.org/10.1007/s00254-005-0010-6>
- Yang J, Cao G, Han D, Yuan H, Hu Y, Shi P, Chen Y (2019) Deformation of the aquifer system under groundwater level fluctuations and its implication for land subsidence control in the Tianjin coastal region. *Environ Monit Assess* 191:162. <https://doi.org/10.1007/s10661-019-7296-4>
- Yao J, Tjuatja S, Huang H (2015) Real-time vibratory strain sensing using passive wireless antenna sensor. *IEEE Sens J* 15:4338–4345. <https://doi.org/10.1109/jsen.2015.2416672>
- Zhang C-C et al (2018) Vertically distributed sensing of deformation using fiber optic sensing. *Geophys Res Lett* 45:11732–11741. <https://doi.org/10.1029/2018gl080428>
- Zhang CC, Shi B, Zhang S, Gu K, Liu SP, Gong XL, Wei GQ (2021a) Microanchored borehole fiber optics allows strain profiling of the shallow subsurface. *Sci Rep* 11:9173. <https://doi.org/10.1038/s41598-021-88526-8>
- Zhang L, Shi B, Zhu H, Yu XB, Han H, Fan X (2021b) PSO-SVM-based deep displacement prediction of Majiagou landslide considering the deformation hysteresis effect. *Landslides* 18:179–193. <https://doi.org/10.1007/s10346-020-01426-2>
- Zhu H-H, Shi B, Zhang C-C (2017) FBG-based monitoring of geohazards: current status and trends. *Sensors* 17:452. <https://doi.org/10.3390/s17030452>
- Zhu JY, Guo HP (2014) Relation between land subsidence and deep groundwater exploitation in Cangzhou city. *Adv Mater Res* 864–867:2213–2217. <https://doi.org/10.4028/www.scientific.net/AMR.864-867.2213>

Publisher's Note Springer Nature remains neutral with regard to jurisdictional claims in published maps and institutional affiliations.